RSC Advances

PAPER

View Article Online
View Journal | View Issue

Cite this: *RSC Adv.*, 2018, **8**, 10389

Received 22nd December 2017
Accepted 8th March 2018

DOI: 10.1039/c7ra13582c

rsc.li/rsc-advances

Highly (100)-oriented $CH_3NH_3PbI_3(Cl)$ perovskite solar cells prepared with NH_4Cl using an air blow method†

Takeo Oku,* Yuya Ohishi and Naoki Ueoka

The effects of adding NH_4Cl *via* an air blow process on $CH_3NH_3PbI_3(Cl)$ perovskite solar cells were investigated. $CH_3NH_3PbI_3(Cl)$ solar cells containing various amounts of NH_4Cl were fabricated by spin-coating. The microstructures of the resulting cells were investigated by X-ray diffraction, optical microscopy, and scanning electron microscopy. The current density–voltage characteristics of the cell were improved by adding an appropriate amount of NH_4Cl and air blowing, which increased the photoconversion efficiency to 14%. Microstructure analysis indicated that the perovskite layer contained dense grains with strong (100) orientation, as a result of NH_4Cl addition and air blowing. The ratio of the (100)/(210) reflection intensities for the perovskite crystals was 2000 times higher than that of randomly oriented grains. The devices were stable when stored in ambient air for two weeks.

Introduction

Thin film solar cells containing methylammonium trihalogenoplumbate(II) ($CH_3NH_3PbI_3$) compounds with perovskite structures have recently been widely studied.[1–4] This has been due to their easy fabrication processes and high photoconversion efficiencies compared with conventional fullerene-based organic solar cells. Conversion efficiencies for these conventional cells have reached 15%,[5] but higher efficiencies have been achieved for various perovskite compounds and device structures.[6–8] Conversion efficiencies above 20% have been reported.[9–18]

The photovoltaic properties of perovskite-based solar cells depend on the composition and crystal structure of the perovskite compound. Introducing metal atoms such as tin (Sn),[19,20] antimony (Sb),[21–25] copper (Cu),[26] arsenic (As),[27] germanium (Ge),[28,29] indium (In),[29] or thallium (Tl)[29] at lead (Pb) sites has been performed. The optical absorption range of perovskite compounds has been extended by Sn or Tl doping.[19,20,29]

Introducing cesium,[10] rubidium,[14] formamidinium ($NH{=}CHNH_3$, FA)[12] or ethylammonium ($CH_3CH_2NH_3$, EA)[30] at methylammonium (CH_3NH_3, MA) sites can also improve conversion efficiencies. Studies on doping with bromine (Br)[12,24] or chlorine (Cl)[31,32] at iodine (I) sites of perovskite crystals have been reported. Doping with Cl reportedly increases the diffusion length, which improves the conversion efficiency.[31,33] Various elemental and molecular dopants at Pb, I, and/or MA sites reportedly affect the photovoltaic properties and microstructures of perovskite-based solar cells.[34]

Photovoltaic properties also strongly depend on the morphology of thin films.[35] A large interfacial area between the perovskite layers and TiO_2 electron transport layers can increase carrier separation, which increases the short circuit current density. Smooth and homogeneous surfaces, interfaces, and grain boundary structures of perovskite layers are expected to result in improved open circuit voltages and fill factors.[36]

The present study investigates the effects of adding NH_4Cl to perovskite $CH_3NH_3PbI_3(Cl)$ photovoltaic devices, using a hot air blow method. NH_4Cl has surfactant properties, so is expected to promote a homogeneous morphology.[37–39] The doped Cl is expected to increase the carrier diffusion length in the perovskite crystals.[31,33] The Cl-doped perovskite crystals are denoted as $CH_3NH_3PbI_3(Cl)$ in the present study. The effects of NH_4Cl addition on the formation of perovskite compounds for photovoltaic cells are investigated by light-induced current density–voltage (*J*–*V*) measurements, incident photon-to-current conversion efficiency (IPCE), X-ray diffraction (XRD), optical microscopy (OM), scanning electron microscopy (SEM), and energy dispersive X-ray spectroscopy (EDS).

Experimental

Materials

All reagents and solvents were used as received. For the compact TiO_2 layer, 0.15 M and 0.30 M TiO_2 precursor solutions were prepared from titanium diisopropoxide bis(acetylacetonate) (Sigma-Aldrich, 0.055 mL and 0.11 mL, respectively) with 1-butanol (1 mL). For the mesoporous TiO_2 layer, TiO_2 paste was prepared using TiO_2 powder (Nippon Aerosil, P-25) with

---

Department of Materials Science, The University of Shiga Prefecture, 2500 Hassaka, Hikone, Shiga 522-8533, Japan. E-mail: oku@mat.usp.ac.jp

† Electronic supplementary information (ESI) available. See DOI: 10.1039/c7ra13582c

poly(ethylene glycol) (Nacalai Tesque, PEG #20000) in ultrapure water. The resulting dispersion was mixed with acetylacetone (Wako Pure Chemical Industries, 10 μL) and Triton X-100 (Sigma-Aldrich, 5 μL), stirred for 30 min, and then left to stand for 12 h to allow bubbles in the mixture to disperse.

For the perovskite layer, a solution containing CH_3NH_3I (Showa Chemical Co., Ltd., 190.7 mg) and $PbCl_2$ (Sigma-Aldrich, 111.2 mg) was prepared with a molar ratio of 3 : 1 in *N*,*N*-dimethylformamide (Nacalai Tesque, 0.5 mL). This solution was then stirred at 60 °C for 24 h.

For the hole transport layer, two solutions of 2,2′,7,7′-tetrakis[*N*,*N*-di(*p*-methoxyphenyl)amino]-9,9′-spirobifluorene (spiro-OMeTAD, Sigma-Aldrich, 36.1 mg) in chlorobenzene (Wako Pure Chemical Industries, 0.5 mL) and lithium bis(trifluoromethylsulfonyl)imide (Li-TFSI, Tokyo Chemical Industry, 260 mg) in acetonitrile (Nacalai Tesque, 0.5 mL) were prepared and stirred for 12 h. The former spiro-OMeTAD solution in chlorobenzene containing 4-*tert*-butylpyridine (Aldrich, 14.4 μL) was mixed with the latter Li-TFSI solution (8.8 μL), and the resulting solution was stirred for 30 min at 70 °C.

Device fabrication

Fig. 1 shows a schematic illustration of the process used to fabricate the $TiO_2/CH_3NH_3PbI_3(Cl)$ photovoltaic cells. Details of the basic fabrication process have been described previously,[39–41] with the exception of details of the air blow procedure. F-doped tin oxide (FTO) substrates were ultrasonically cleaned with acetone and methanol, and then dried under nitrogen gas. The 0.15 M TiO_2 precursor solution was spin-coated on the FTO substrate at 3000 rpm for 30 s, and the coated substrate was then heated to 125 °C for 5 min in air to form a TiO_x layer.

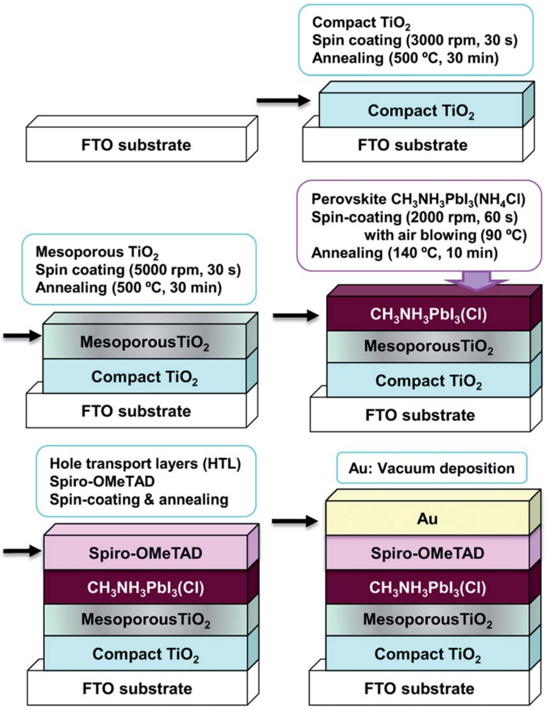

Fig. 1 Schematic illustration of the process used to fabricate the $CH_3NH_3PbI_3(Cl)$ photovoltaic cells.

The 0.30 M TiO_2 precursor solution was spin-coated onto the TiO_x layer at 3000 rpm for 30 s, and the coated substrate was then heated at 125 °C for 5 min. This process of coating with 0.30 M solution was performed a second time, and the resulting FTO substrate was then annealed at 500 °C for 30 min to form a compact TiO_2 layer. For the mesoporous TiO_2 layer, the TiO_2 paste was spin-coated onto the substrate at 5000 rpm for 30 s. The substrate was then annealed at 120 °C for 5 min, and then at 500 °C for 30 min, to form a mesoporous TiO_2 layer.

Then, a solution containing $CH_3NH_3PbI_3(Cl)$ was introduced into the TiO_2 mesopores of the above coated substrate by the spin-coating method.[42–44] For the spin-coating procedure, air blowing at a rate of 6 m s^{-1} and 3300 cm^3 s^{-1} was applied perpendicular to the substrate at a temperature of 90 °C for 60 s, as indicated in Fig. 1. The resulting substrate was annealed at 140 °C for 10 min to form the perovskite layer.[40]

A hole transport layer was then prepared by spin-coating onto the perovskite layer. All procedures for preparing thin films were performed in ambient air at a temperature of 28 °C and humidity of ~50%. Finally, a gold (Au) thin film was evaporated onto the hole transport layer, as the top metal electrode. The layered structure of the solar cell was denoted $FTO/TiO_2/CH_3NH_3PbI_3(Cl)$/spiro-OMeTAD/Au, as shown in Fig. 1.

Characterization

The *J*–*V* characteristics of the photovoltaic cells were measured under illumination at 100 mW cm^{-2}, using an AM 1.5 solar simulator (San-ei Electric, XES-301S). *J*–*V* measurements were performed using a source measure unit (Keysight, B2901A Precision SMU). The scan rate and sampling time were ~0.08 V s^{-1} and 1 m s, respectively. Four cells were tested for each cell composition. The solar cells were illuminated through the sides of the FTO substrates, and the illuminated area was 0.090 cm^2. IPCE of the cells were also measured (Enli Technology, QE-R). The microstructures of the cells were investigated using an X-ray diffractometer (Bruker, D2 PHASER), a transmission optical microscope (Nikon, Eclipse E600), and a scanning electron microscope (Jeol, JSM-6010PLUS/LA) equipped with EDS.

Results and discussion

Fig. 2 shows the *J*–*V* characteristics of the $TiO_2/CH_3NH_3PbI_3(Cl)$/spiro-OMeTAD photovoltaic cells under illumination, in which the effects of NH_4Cl addition are evident. Forward and reverse scans are indicated by the dotted and solid lines, respectively. The measured photovoltaic parameters of the $TiO_2/CH_3NH_3PbI_3(Cl)$ cells are summarized in Table 1, and forward (Fw) and reverse (Rv) values are listed. Small hysteresis between the forward and reverse scans is observed for the *J*–*V* characteristics in Fig. 2, and the degree of hysteresis decreases with NH_4Cl addition. A small amount of carriers may have been generated

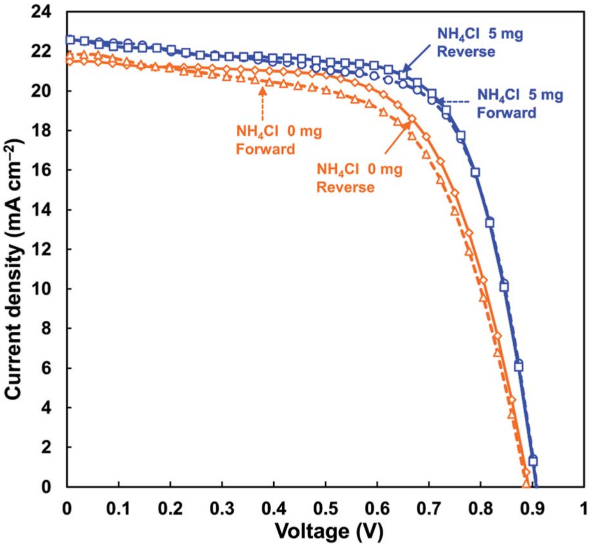

Fig. 2 *J*–*V* characteristics of $CH_3NH_3PbI_3(Cl)$ solar cells with and without NH_4Cl.

and transported into the TiO_2 layer during the *J*–*V* measurements (*i.e.* during light irradiation and subsequent current flow). In this case, the electrical resistance would decrease and the photocurrent would increase, resulting in the hysteresis. The perovskite would also exhibit hysteresis properties in its *J*–*V* characteristics.[45]

The $CH_3NH_3PbI_3(Cl)$ cell without NH_4Cl provides a power conversion efficiency (η) of 12.41% for the reverse scan. The average efficiency (η_{ave}) of four electrodes in identical cells is 12.37%, as shown in Table 1. The short-circuit current density (J_{SC}), open-circuit voltage (V_{OC}) and fill factor (FF) are all higher for the NH_4Cl-added $CH_3NH_3PbI_3(Cl)$ cells, which results in the increases in their η values. Adding 5 mg of NH_4Cl yields the highest efficiency $CH_3NH_3PbI_3(Cl)$ cell, with a η of 14.03%, FF of 0.685, J_{SC} of 22.6 mA cm^{-2}, and V_{OC} of 0.908 V. The highest average power conversion efficiency (η_{ave}) of 13.74% is obtained for this cell. The series resistance (R_s) also decreases with NH_4Cl addition (Table 1), leading to an increase in the J_{SC}. After standing for two weeks in ambient air, the decreases in efficiencies of cells containing NH_4Cl are small. A η of 13.19% is still obtained, as shown in Table 2.

IPCE spectra of the $CH_3NH_3PbI_3(Cl)$ devices were shown in Fig. 3. The $CH_3NH_3PbI_3(Cl)$ cells show photoconversion efficiencies between 320 and 810 nm, which corresponds to an energy gap of 1.53 eV for the $CH_3NH_3PbI_3$. The IPCE was improved in the range of 400–700 nm by adding NH_4Cl, which lead to the increase of J_{SC} values. Although the J_{SC} values should agree with the integrated values of IPCE as previously reported in alkali metal-doped perovskite solar cells,[46] the J_{SC} values in the present work is slightly lower than the integrated values of IPCE. In order to measure the IPCE of the perovskite solar cells, DC measurements mode is better. However, the lowest frequency of the lock-in-amplifier in the present work is 4 Hz (QE-R, Enli Technology), and the lower IPCE values tended to be measured compared with the actual IPCE values. Therefore, only the wavelength region can be evaluated for the IPCE data in the present work.

OM images of the $CH_3NH_3PbI_3(Cl)$ cells are shown in Fig. 4. Microparticles with sizes of 5–10 μm are observed for the cell prepared without NH_4Cl, as shown in Fig. 4(a). Adding NH_4Cl to the $CH_3NH_3PbI_3(Cl)$ decreases the particle size, as shown in Fig. 4(b)–(d). In addition, networking structures with sizes of ~10 μm between microparticles are observed, especially in Fig. 4(d). These networking microstructures could potentially improve the photovoltaic properties.

A SEM image of the $CH_3NH_3PbI_3(Cl)$ cell without NH_4Cl is shown in Fig. 5(a). Microparticles with sizes of 5–10 μm are observed on the surface of the mesoporous TiO_2, which correspond to those in Fig. 4(a). The particles appear have crystal facets. EDS elemental mapping images of the Pb M line, I L line, Cl K line, C K line, and N K line are shown in Fig. 5(b)–(f), respectively. These elemental mapping images indicate that the particles observed in Fig. 5(a) correspond to the $CH_3NH_3PbI_3$ compound. The Pb and I compositions and C : N ratio were calculated from the EDS spectrum using background correction by normalizing the peaks, and are listed in Table 3. Although the EDS values contain some errors, these results seem to

Table 2 Measured photovoltaic parameters of the $CH_3NH_3PbI_3(Cl)$ solar cells after two weeks

NH_4Cl (mg)	J_{SC} (mA cm^{-2})	V_{OC} (V)	FF	η (%)	R_s (Ω cm^{-2})
0	20.5	0.870	0.647	11.51	4.61
1	21.6	0.892	0.640	12.34	4.51
3	22.1	0.893	0.668	13.19	4.63
5	21.5	0.893	0.643	12.33	4.29

Table 1 Measured photovoltaic parameters of the $CH_3NH_3PbI_3(Cl)$ solar cells

NH_4Cl (mg)	Scan	J_{SC} (mA cm^{-2})	V_{OC} (V)	FF	η (%)	η_{ave} (%)	R_s (Ω cm^{-2})
0	Fw	21.8	0.889	0.610	11.85	11.76	6.92
	Rv	21.5	0.893	0.647	12.41	12.37	6.56
1	Fw	22.4	0.909	0.633	12.90	12.50	6.44
	Rv	22.2	0.912	0.651	13.19	12.89	6.18
3	Fw	22.4	0.913	0.636	13.01	11.25	6.40
	Rv	22.5	0.917	0.651	13.40	12.13	6.06
5	Fw	22.6	0.908	0.673	13.83	13.59	4.66
	Rv	22.6	0.908	0.685	14.03	13.74	4.70

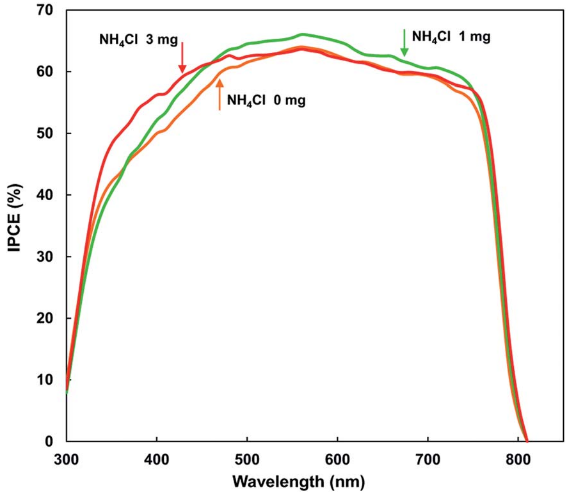

Fig. 3 IPCE spectra of $CH_3NH_3PbI_3(Cl)$ solar cells with and without NH_4Cl.

indicate that the composition of $CH_3NH_3PbI_3$ may be I deficient. In addition, EDS indicates that C is dispersed throughout the matrix.

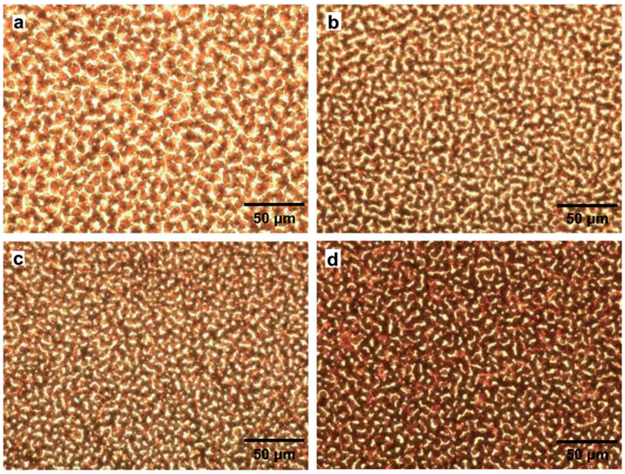

Fig. 4 OM images of $CH_3NH_3PbI_3(Cl)$ cells containing (a) 0 mg, (b) 1 mg, (c) 3 mg, and (d) 5 mg of NH_4Cl.

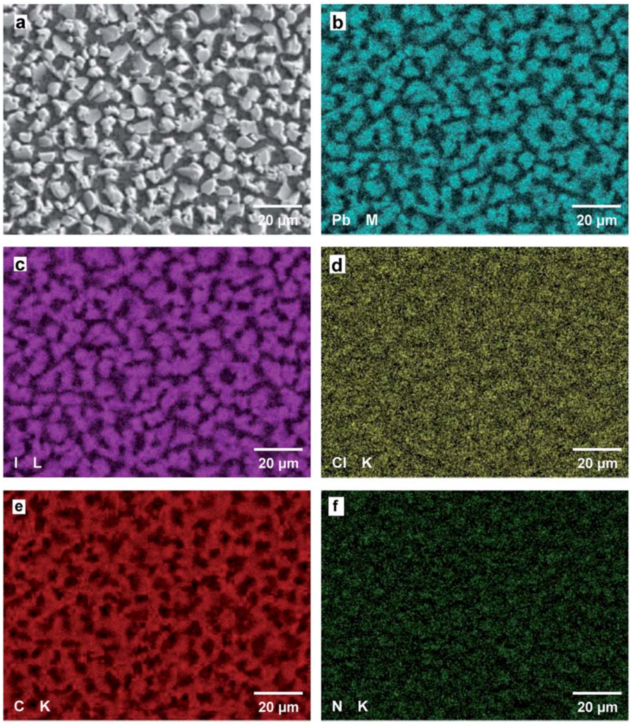

Fig. 5 (a) SEM image of the $CH_3NH_3PbI_3(Cl)$ cell without NH_4Cl, and corresponding elemental mapping images of the (b) Pb M line, (c) I L line, (d) Cl K line, (e) C K line, and (f) N K line.

Fig. 6(a) shows a SEM image of the $CH_3NH_3PbI_3(Cl)$ cell containing 5 mg of NH_4Cl. The surface morphology changes upon adding NH_4Cl to the $CH_3NH_3PbI_3$. The average particle sizes is ~5 μm, and crystals are connected to each other with special facets. These networking surface structures could potentially improve the surface coverage and therefore the photovoltaic properties. Fig. 6(b)–(f) show EDS elemental mapping images of Pb, I, Cl, C, and N, respectively. The elemental compositions and C : N ratios were calculated from the EDS spectra, and are also listed in Table 3. These data indicate that the $CH_3NH_3PbI_3$ starting composition may be I deficient. Cl would be doped into the $CH_3NH_3PbI_3$, as shown in Table 3. In Fig. 6(e), C appears to be dispersed throughout the matrix. The EDS results indicate that the I site occupancy would be <1, and that this I deficiency may increase the hole concentration. The networking surface structures are expected to affect the photovoltaic properties, in addition to the doping effect of Cl at I sites. The $CH_3 : NH_3$ ratio in the $CH_3NH_3PbI_3(Cl)$ phase prepared by air blowing is almost 6 : 4. This is consistent with excess CH_3 compared with NH_3, and is caused by the air blowing procedure as shown in Table 3. Although the EDS values contain some errors, these results seem to indicate that the composition of $CH_3NH_3PbI_3$ may be I deficient. In addition, EDS indicates that C is dispersed throughout the matrix.

Fig. 7(a)–(d) shows XRD patterns of the $FTO/TiO_2/CH_3NH_3PbI_3(Cl)$/spiro-OMeTAD/Au cells. The diffraction peaks can be indexed by a cubic crystal system ($Pm\bar{3}m$) for $CH_3NH_3PbI_3(Cl)$ perovskite thin films. The XRD pattern of a $CH_3NH_3PbI_3(Cl)$ cell prepared without air blowing or $PbCl_2$ is shown in Fig. 7(e). The diffraction peaks of FTO and TiO_2 arise from the FTO substrate and TiO_2 mesoporous layer, respectively. For ordinary $CH_3NH_3PbI_3$ cells prepared at 100 °C without air blowing, XRD

Table 3 Compositions of the solar cells as measured by EDS[a]

NH_4Cl (mg)	Pb (at%)	I (at%)	Cl (at%)	C : N (at%)
0	33.5	61.2	5.3	61.9 : 38.1
1	33.5	61.9	4.6	61.7 : 38.3
3	34.0	61.6	4.5	61.8 : 38.2
5	33.7	60.8	5.5	61.8 : 38.2
5[a]	33.5	61.8	4.7	52.0 : 48.0

[a] No air blowing or $PbCl_2$.

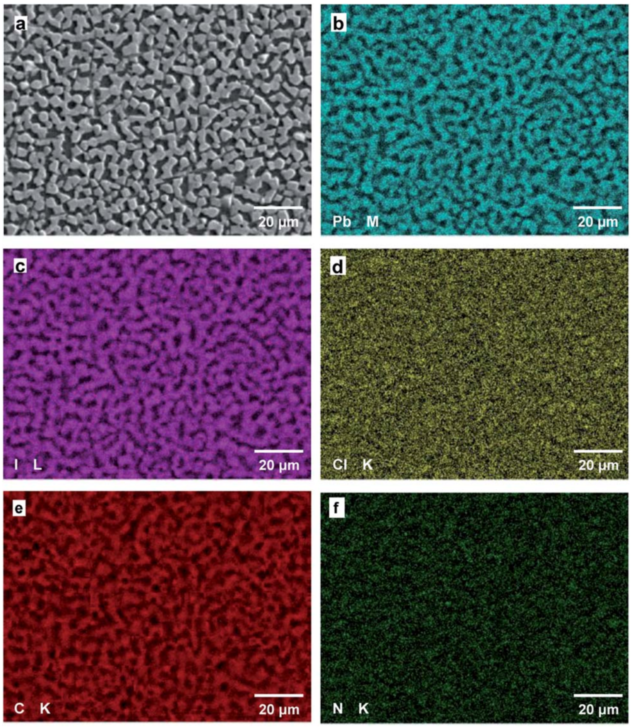

Fig. 6 (a) SEM image of the $CH_3NH_3PbI_3(Cl)$ cell containing 5 mg of NH_4Cl, and corresponding elemental mapping images of the (b) Pb M line, (c) I L line, (d) Cl K line, (e) C K line, and (f) N K line.

peaks of PbI_2 have been reported[41] similarly to those in Fig. 7(e). The intensities of the 100 and 200 peaks of the perovskite phase increase by more than 100 times with air blowing and NH_4Cl, as observed in Fig. 7(b)–(d). The 100 and 200 reflections are sufficiently intense that the diffraction peaks of FTO and TiO_2 are not readily apparent.

The ratios of the 100 diffraction intensities (I_{100}) to the 210 diffraction intensities (I_{200}) of the perovskite crystals were calculated as I_{100}/I_{210}, from the XRD data in Fig. 6. The results are summarized in Table 4. If the $CH_3NH_3PbI_3$ cubic perovskite particles are randomly oriented, then the I_{100}/I_{210} value should be 1.81.[34] For the cell prepared using air blowing and without NH_4Cl, the I_{100}/I_{210} is 61. This indicates that the (100) planes of the perovskite particles are preferentiality oriented parallel to the FTO substrate. Adding NH_4Cl to the cell results in the I_{100}/I_{210} increasing to 3600, which is 2000 times higher than the I_{100}/I_{210} of randomly oriented perovskite crystals. The cell prepared with 5 mg of NH_4Cl without air blowing or $PbCl_2$ has an I_{100}/I_{210} of 2.8. This indicates that most of the perovskite particles are randomly oriented. The ratios of the I_{100} intensities to the FTO substrate intensities (I_{FTO}) were also calculated for the perovskite crystals, and are also shown in Table 4. Using air blowing and NH_4Cl increases the I_{100}/I_{FTO}. These results indicate that preferential (100) crystal orientation occurs in films prepared using air blowing with NH_4Cl. By using a least squares method, the lattice constants were determined to be 6.274, 6.276, 6.276, 6.276, and 6.275 Å for the cells with NH_4Cl 0 mg, 1 mg, 3 mg, 5 mg, and 5 mg without air blow, respectively, and the lattice constants are almost constant for the cell.

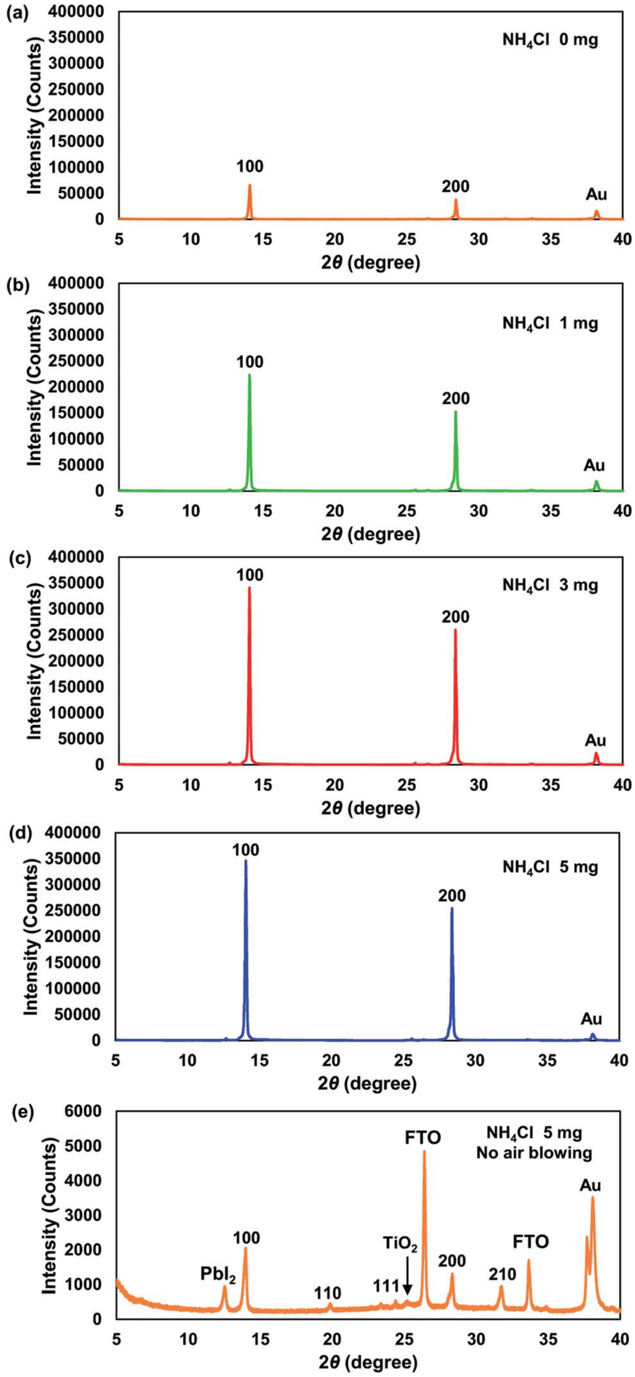

Fig. 7 XRD patterns of $CH_3NH_3PbI_3(Cl)$ cells containing (a) 0 mg, (b) 1 mg, (c) 3 mg, and (d) 5 mg of NH_4Cl, and (e) XRD pattern of the $CH_3NH_3PbI_3(Cl)$ cell containing 5 mg of NH_4Cl without air blowing.

Two mechanisms are considered for the formation of the (100)-oriented $CH_3NH_3PbI_3(Cl)$ perovskite crystals. The first mechanism is crystal growth being promoted by air blowing during spin-coating of the perovskite layers. When the $CH_3NH_3PbI_3(Cl)$ solution crystalizes into perovskite particles, fast annealing with air flow accelerates the crystallization of

Table 4 Ratios of 100 diffraction intensities (I_{100}) to 210 diffraction intensities (I_{200}) and FTO substrate diffraction intensities (I_{FTO}), for the perovskite crystals

+NH_4Cl (mg)	I_{100}/I_{210}	I_{100}/I_{FTO}
Calculation[a]	1.8	—
0	69	51
1	510	170
3	3400	280
5	3600	270
5[b]	2.8	0.40

[a] Calculated from randomly oriented cubic $CH_3NH_3PbI_3$ crystals. [b] No air blowing or $PbCl_2$.

$CH_3NH_3PbI_3(Cl)$. The (100) planes of the perovskite crystals have low surface tension, which results in the growth of (100)-oriented crystals. When highly-oriented crystals are formed, the amount of high angle grain boundaries decreases, which decreases the R_s and increases the V_{OC}. The second mechanism is the formation of a homogeneous morphology during annealing, as a result of the NH_4Cl surfactant. Networking structures are formed in cells containing NH_4Cl, as observed in Fig. 4(d). This improves the surface coverage and carrier transport, which increases the FF and J_{SC}. The improved conversion efficiency can be described by these two mechanisms.

Cl doping at I sites also promotes the photovoltaic properties of the cells. Excess $2(CH_3NH_3Cl)$ could be vaporized from the starting composition of $3(CH_3NH_3I)$ + $PbCl_2$.[42–44] A small amount of residual Cl is doped into the $CH_3NH_3PbI_3$ phase, as detected by EDS. The increases the exciton diffusion length,[31,33] which increases the J_{SC}. Further investigation is required regarding the specific nanostructures in the cell.

Conclusions

The effects of NH_4Cl addition using an air blow method on $CH_3NH_3PbI_3(Cl)$ perovskite solar cells were investigated. The *J–V* characteristics were improved by introducing an appropriate amount of NH_4Cl and air blowing. The resulting cell conversion efficiency was 14%. Microstructure analysis by XRD, OM, SEM, and EDS indicated that highly (100)-orientated perovskite crystals with dense grains were formed when using NH_4Cl and air blowing. The I_{100}/I_{210} ratio of the perovskite crystals was 2000 times higher than that of randomly oriented grains. The (100)-oriented cells were stable during storage for two weeks in ambient air. Formation of the (100)-oriented perovskite crystals was due to the crystal growth accelerated by air blowing during spin-coating. The highly-oriented crystals with decreased grain boundaries could decrease the R_s and increase the V_{OC}. In addition, formation of a homogeneous morphology with networking structures was promoted by the NH_4Cl surfactant. Improvement of the surface coverage and carrier transport increased the FF and J_{SC}. As a result, these microstructures improved the conversion efficiency, and this NH_4Cl addition combined with an air blow method is an effective method for fabrication of highly crystalline-oriented homogeneous thin films.

Conflicts of interest

There are no conflicts to declare.

Acknowledgements

This research was supported in part by the Satellite Cluster Program of the Japan Science and Technology Agency. The authors thank A. Suzuki and M. Fukaya of The University of Shiga Prefecture, Japan, for their invaluable support. They also thank Aidan G. Young, PhD, from Edanz Group (www.edanzediting.com/ac) for editing a draft of this manuscript.

References

1 A. Kojima, K. Teshima, Y. Shirai and T. Miyasaka, *J. Am. Chem. Soc.*, 2009, **131**, 6050–6051.
2 J.-H. Im, C.-R. Lee, J.-W. Lee, S.-W. Park and N.-G. Park, *Nanoscale*, 2011, **3**, 4088–4093.
3 H. S. Kim, C. R. Lee, J. H. Im, K. B. Lee, T. Moehl, A. Marchioro, S. J. Moon, R. Humphry-Baker, J. H. Yum, J. E. Moser, M. Grätzel and N. G. Park, *Sci. Rep.*, 2012, **2**, 591–597.
4 M. M. Lee, J. Teuscher, T. Miyasaka, T. N. Murakami and H. J. Snaith, *Science*, 2012, **338**, 643–647.
5 J. Burschka, N. Pellet, S. J. Moon, R. Humphry-Baker, P. Gao, M. K. Nazeeruddin and M. Grätzel, *Nature*, 2013, **499**, 316–320.
6 H. Zhou, Q. Chen, G. Li, S. Luo, T.-B. Song, H.-S. Duan, Z. Hong, J. You, Y. Liu and Y. Yang, *Science*, 2014, **345**, 542–546.
7 G. Fu, L. Hou, Y. Wang, X. Liu, J. Wang, H. Li, Y. Cui, D. Liu, X. Li and S. Yang, *Sol. Energy Mater. Sol. Cells*, 2017, **165**, 36–44.
8 J. Zheng, M. Zhang, C. F. J. Lau, X. Deng, J. Kim, Q. Ma, C. Chen, M. A. Green, S. Huang and A. W. Y. Ho-Baillie, *Sol. Energy Mater. Sol. Cells*, 2017, **168**, 165–171.
9 W. S. Yang, J. H. Noh, N. J. Jeon, Y. C. Kim, S. Ryu, J. Seo and S. I. Seok, *Science*, 2015, **348**, 1234–1237.
10 M. Saliba, T. Matsui, J. Y. Seo, K. Domanski, J. P. Correa-Baena, M. K. Nazeeruddin, S. M. Zakeeruddin, W. Tress, A. Abate, A. Hagfeldtd and M. Grätzel, *Energy Environ. Sci.*, 2016, **9**, 1989–1997.
11 M. Saliba, S. Orlandi, T. Matsui, S. Aghazada, M. Cavazzini, J. P. Correa-Baena, P. Gao, R. Scopelliti, E. Mosconi, K. H. Dahmen, F. De Angelis, A. Abate, A. Hagfeldt, G. Pozzi, M. Graetzel and M. K. Nazeeruddin, *Nat. Energy*, 2016, **1**, 15017.
12 D. Bi, W. Tress, M. I. Dar, P. Gao, J. Luo, C. Renevier, K. Schenk, A. Abate, F. Giordano, J. P. C. Baena, J. D. Decoppet, S. M. Zakeeruddin, M. K. Nazeeruddin, M. Grätzel and A. Hagfeldt, *Sci. Adv.*, 2016, **2**, 1501170.

13 D. Bi, C. Yi, J. Luo, J.-D. Décoppet, F. Zhang, S. M. Zakeeruddin, X. Li, A. Hagfeldt and M. Grätzel, *Nat. Energy*, 2016, **1**, 16142.

14 M. Saliba, T. Matsui, K. Domanski, J.-Y. Seo, A. Ummadisingu, S. M. Zakeeruddin, J.-P. Correa-Baena, W. R. Tress, A. Abate, A. Hagfeldt and M. Grätzel, *Science*, 2016, **354**, 206–209.

15 M. He, B. Li, X. Cui, B. Jiang, Y. He, Y. Chen, D. O'Neil, P. Szymanski, M. A. EI-Sayed, J. Huang and Z. Lin, *Nat. Commun.*, 2017, **8**, 16045.

16 S. S. Shin, E. J. Yeom, W. S. Yang, S. Hur, M. G. Kim, J. Im, J. Seo, J. H. Noh and S. I. Seok, *Science*, 2017, **356**, 167–171.

17 Z. Tang, T. Bessho, F. Awai, T. Kinoshita, M. M. Maitani, R. Jono, T. N. Murakami, H. Wang, T. Kubo, S. Uchida and H. Segawa, *Sci. Rep.*, 2017, **7**, 12183.

18 J.-M. Wang, Z.-K. Wang, M. Li, C.-C. Zhang, L.-L. Jiang, K.-H. Hu, Q.-Q. Ye and L.-S. Liao, *Adv. Energy Mater.*, 2017, **7**, 1701688.

19 F. Hao, C. C. Stoumpos, D. H. Cao, R. P. H. Chang and M. G. Kanatzidis, *Nat. Photonics*, 2014, **8**, 489–494.

20 W. Liao, D. Zhao, Y. Yu, N. Shrestha, K. Ghimire, C. R. Grice, C. Wang, Y. Xiao, A. J. Cimaroli, R. J. Ellingson, N. J. Podraza, K. Zhu, R.-G. Xiong and Y. Yan, *J. Am. Chem. Soc.*, 2016, **138**, 12360–12363.

21 T. Oku, Y. Ohishi and A. Suzuki, *Chem. Lett.*, 2016, **45**, 134–136.

22 T. Oku, Y. Ohishi, A. Suzuki and Y. Miyazawa, *Metals*, 2016, **6**, 147.

23 J. Zhang, M. H. Shang, P. Wang, X. Huang, J. Xu, Z. Hu, Y. Zhu and L. Han, *ACS Energy Lett.*, 2016, **1**, 535–541.

24 T. Oku, Y. Ohishi and A. Suzuki, *AIP Conf. Proc.*, 2017, **1807**, 020007.

25 Y. Ando, T. Oku and Y. Ohishi, *Jpn. J. Appl. Phys.*, 2018, **57**, 02CE02.

26 Y. Shirahata and T. Oku, *Phys. Status Solidi A*, 2017, **214**, 1700268.

27 A. Hamatani, Y. Shirahata, Y. Ohishi, M. Fukaya and T. Oku, *Adv. Mater. Phys. Chem.*, 2017, **7**, 1–10.

28 T. Krishnamoorthy, H. Ding, C. Yan, W. L. Leong, T. Baikie, Z. Zhang, M. Sherburne, S. Li, M. Asta, N. Mathews and S. G. Mhaisalkar, *J. Mater. Chem. A*, 2015, **3**, 23829–23832.

29 Y. Ohishi, T. Oku and A. Suzuki, *AIP Conf. Proc.*, 2016, **1709**, 020020.

30 W. Peng, X. Miao, V. Adinolfi, E. Alarousu, O. El Tall, A. H. Emwas, C. Zhao, G. Walters, J. Liu, O. Ouellette, J. Pan, B. Murali, E. H. Sargent, O. F. Mohammed and O. M. Bakr, *Angew. Chem., Int. Ed.*, 2016, **55**, 10686–10690.

31 S. D. Stranks, G. E. Eperon, G. Grancini, C. Menelaou, M. J. P. Alcocer, T. Leijtens, L. M. Herz, A. Petrozza and H. J. Snaith, *Science*, 2013, **342**, 341–344.

32 T. Oku, K. Suzuki and A. Suzuki, *J. Ceram. Soc. Jpn.*, 2016, **124**, 234–238.

33 Q. Dong, Y. Fang, Y. Shao, P. Mulligan, J. Qiu, L. Cao and J. Huang, *Science*, 2015, **347**, 967–970.

34 T. Oku, *Solar Cells and Energy Materials*, Walter de Gruyter, Berlin, 2017.

35 W. Nie, H. Tsai, R. Asadpour, J. C. Blancon, A. J. Neukirch, G. Gupta, J. J. Crochet, M. Chhowalla, S. Tretiak, M. A. Alam, H. L. Wang and A. D. Mohite, *Science*, 2015, **347**, 522–525.

36 J.-W. Lee, S.-H. Bae, N. D. Marco, Y. T. Hsieh, Z. Dai and Y. Yang, *Materials Today Energy*, 2018, **7**, 149–160.

37 C. Zuo and L. Ding, *Nanoscale*, 2014, **6**, 9935–9938.

38 J. He and T. Chen, *J. Mater. Chem. A*, 2015, **3**, 18514–18520.

39 T. Oku, Y. Ohishi, A. Suzuki and Y. Miyazawa, *J. Ceram. Soc. Jpn.*, 2017, **125**, 303–307.

40 T. Oku and Y. Ohishi, *J. Ceram. Soc. Jpn.*, 2018, **126**, 56.

41 T. Oku, M. Zushi, Y. Imanishi, A. Suzuki and K. Suzuki, *Appl. Phys. Express*, 2014, **7**, 121601.

42 H. Yu, F. Wang, F. Xie, W. Li, J. Chen and N. Zhao, *Adv. Funct. Mater.*, 2014, **24**, 7102–7108.

43 A. Dualeh, N. Tétreault, T. Moehl, P. Gao, M. K. Nazeeruddin and M. Grätzel, *Adv. Funct. Mater.*, 2014, **24**, 3250–3258.

44 J. A. McLeod, Z. Wu, B. Sun and L. Liu, *Nanoscale*, 2016, **8**, 6361–6368.

45 H. J. Snaith, A. Abate, J. M. Ball, G. E. Eperon, T. Leijtens, N. K. Noel, S. D. Stranks, J. T.-W. Wang, K. Wojciechowski and W. Zhang, *J. Phys. Chem. Lett.*, 2014, **5**, 1511–1515.

46 Z. Tang, S. Uchida, T. Bessho, T. Kinoshita, H. Wang, F. Awai, R. Jono, M. M. Maitani, J. Nakazaki, T. Kubo and H. Segawa, *Nano Energy*, 2018, **45**, 184–192.